Response to reviewer#1

Thanks for the reviewer's helpful suggestions! The comments are addressed point-by-point and responses are listed below.

Comment: General comments: Uncertainty of aerosol optical properties causes further uncertainties in climate prediction in model simulations, in which the real part of the refractive index is important. Thus, determining the aerosol real part of refractive index (RRI) is an important issue.

Reply: We thank the anonymous reviewer's comments.

Comment: The manuscript entitled "A new parameterization scheme of the real part of the ambient aerosols refractive index" studied the RRI by field measurement in East China. The title is "A new parameterization scheme of the real part of : : :.", however, as I understood, the parameter scheme is just established by the measurements of the system reported by Zhao et al., (2018b). Moreover, the universality of this parameterization scheme at other location is unknown.

Reply： Thanks for the comment. The objective of this article is to bring up a novel idea of parameterization scheme of real part of the refractive index (RRI) for ambient aerosol. Traditionally, RRI is parameterized by the measurement of ambient aerosol main inorganic components (Han et al., 2009). The influence of organic compositions is ignored. In this work, we found that the ambient aerosol RRI was highly related with the aerosol effective density (ρ_{eff}) rather than the chemical components. Thus, a new parameterization scheme of the RRI using the effective density was proposed.

To validate the universality of this parameterization scheme, we conducted another measurement in the campus of Peking University (PKU) (N39°59′, E116°18′), in China, where the aerosol effective density and real part of the refractive index are measured concurrently at 16th, December in 2018. The RRI were also calculated using the parameterization scheme, $\frac{RRI^2-1}{RRI^2+2} = 0.18\rho_{eff}$. Comparison of the measured and calculated RRI is shown in fig. R1. Results show that the calculated and measured RRI agree well.

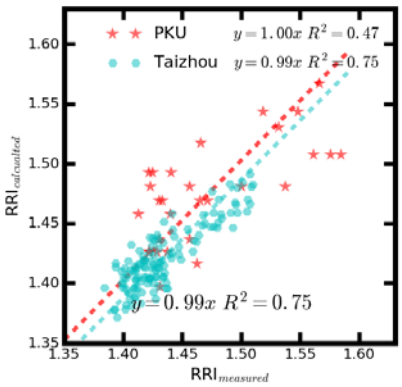

Fig. R1. Comparison between the measured and calculated RRI at PKU and Taizhou.

Comment: Also, the figures and descriptions need be reorganized carefully. Therefore, although this paper focused on the interesting question, it needs further analysis, reorganization, discussion and clarification to improve the confidence of the results.

Reply: We thank the anonymous reviewer's comments and suggestions. We have replotted some figures (1, 2, 5 and 6). We also made some revisions at the introduction and discussion sections in the text.

Comment: Specific comments: 1. Line 26, "reginal" should be "regional".

Reply: Thanks for the comment and we revised it.

Comment: 2. The logics and description of Section "Introduction" are insufficient.

Reply: Thanks for the comment. We have rewritten the introduction and added some descriptions about our work.

Comment: 3. I suggest the authors combine some figures, for example, Figure 1, of the supplement into the main of manuscript.

Reply: Thanks for the comment. Fig. 1 is replotted.

Comment: 4. Line 153-155, the description of variables in equation (5) is confused.

Reply: Thanks for the comment. We added some descriptions in the text. DARF at the TOA is defined as the difference between radiative flux under aerosol-free conditions and aerosol present conditions:

$$\mathrm{DARF} = (f_a\downarrow - f_a\uparrow) - (f_n\downarrow - f_n\uparrow) \quad (5),$$

where $f_a\downarrow$ and $f_a\uparrow$ are the downward and upward radiative irradiance with aerosol present conditions respectively; the difference between $f_a\downarrow$ and $f_a\uparrow$

($f_a\downarrow - f_a\uparrow$) is the downward radiative irradiance flux with aerosol present conditions; $f_n\downarrow$ and $f_n\uparrow$ correspond to the downward and upward radiative irradiance values under aerosol free conditions respectively; the difference between $f_n\downarrow$ and $f_n\uparrow$ ($f_n\downarrow - f_n\uparrow$) is the downward radiative irradiance flux for aerosol-free conditions (Kuang et al., 2016).

Comment: 5. Line 152 and Line 234, all of two equations are denoted as (5).
Reply: Thanks for the comment. We have changed the labels for equations.

Comment: 6. Why not use the vertical profiles of temperature, pressure and water vapor at the times corresponding to the aerosol measurements?
Reply: Thanks for the comment. When estimating the aerosol DARF using the SBDART model, the profiles of temperature, pressure, water vapor and the aerosol vertical profiles are necessary. DARF would be different for different vertical profiles of temperature, pressure and water vapor. In this study, we focus on the influence of aerosol RRI variation on the variations in DARF. The profiles of aerosol temperature, pressure, water vapor should be hold constant. Therefore, we use the mean result of the measured radiosonde profile during the field.

Comment: 7. Line 234, what is the meaning of in Equation (5)?
Reply: Thanks for the comment. We have changed the equation into $\mathrm{RRI} = \sqrt{\frac{1+0.36\rho_{eff}}{1-0.18\rho_{eff}}}$, which means that the specific refractive index Re is directly related to aerosol density.

Comment: 8. Can this method be used at other location and other time?
Reply: Thanks for the comment. We have conducted another measurement in Beijing (N39°59′, E116°18′), China, where the aerosol effective density and real part of the refractive index are measured concurrently at 16th, December in 2018. The relationships of the effective density and real part of refractive index are shown in fig. R1. From fig. R1, the results in Beijing agree well with that of Taizhou.

Comment: 9. Why do the authors compare a result with other at different time series and measurement site? So, a reliable result should be induced here to evaluate this study.
Reply: Thanks for the comment. We compare the result with that of Liu and Daum (2008) to demonstrate that their parameterization scheme proposed is not applicable in China. The study of Liu and Daum (2008) is currently the only work that have tried to bridge the effective density and real part of refractive index. The effective density and RRI in their work were estimated using the aerosol chemical components but not the in-situ measurements of effective density and RRI. At the same time, the influence of organic aerosols components on aerosol RRI is not considered in their work.

Comment: 10. In Section 3.1, what's the relation among the wind speed, T and RH with the scattering coefficient and mBC? Which should be reflected in descriptions. Otherwise, the results of meteorology measurements are meaningless.

Reply: Thanks for the comment. The corresponding contents were removed from the text.

Han, Y., Lü, D., Rao, R., Wang, Y. (2009) Determination of the complex refractive indices of aerosol from aerodynamic particle size spectrometer and integrating nephelometer measurements. Applied Optics 48, 4108-4117.

Kuang, Y., Zhao, C.S., Tao, J.C., Bian, Y.X., Ma, N. (2016) Impact of aerosol hygroscopic growth on the direct aerosol radiative effect in summer on North China Plain. Atmospheric Environment 147, 224-233.

Liu, Y., Daum, P.H. (2008) Relationship of refractive index to mass density and self-consistency of mixing rules for multicomponent mixtures like ambient aerosols. Journal of Aerosol Science 39, 974-986.

Response to reviewer#2

Thanks for the reviewer's helpful suggestions! The comments are addressed point-by-point and responses are listed below.

Comment: General comments: The real part of the refractive index is surely still uncertain and its impact on the aerosol radiative forcing (ARF) is large. The scope of this manuscript is important. The logic of this manuscript is generally clear, but the following three points should be clarified.

Reply: Thanks for the comments.

Comment: Firstly, the title is "A new parameterization scheme of the real part of the ambient aerosols refractive index", so the proposed parameterization must be evaluated in the manuscript, but the evaluation is not enough. The parameterization is based on the measurements at one Chinese site during May-June of the specific year. Generally, the parameterization must be universal, so the proposed one should be tested under various conditions using other measurements at different places and seasons or using a numerical model. Otherwise, I suppose other people do not tend to use the proposed parameterization

Reply： Thanks for the comment. The objective of this article is to bring up a novel idea of parameterization scheme of real part of the refractive index (RRI) for ambient aerosol. Traditionally, RRI is parameterized by the measurement of ambient aerosol main inorganic components (Han et al., 2009). The influence of organic compositions is ignored. In this work, we found that the ambient aerosol RRI was highly related with the aerosol effective density (ρ_{eff}) rather than the chemical components. Thus, a new parameterization scheme of the RRI using the effective density was proposed.

To validate the universality of this parameterization scheme, we conducted another measurement in the campus of Peking University (PKU) (N39°59′, E116°18′), in China, where the aerosol effective density and real part of the refractive index are measured concurrently at 16th, December in 2018. The RRI were also calculated using

the parameterization scheme, $\frac{RRI^2-1}{RRI^2+2} = 0.18\rho_{eff}$. Comparison of the measured and calculated RRI is shown in fig. R1. Results show that the calculated and measured RRI show good consistence.

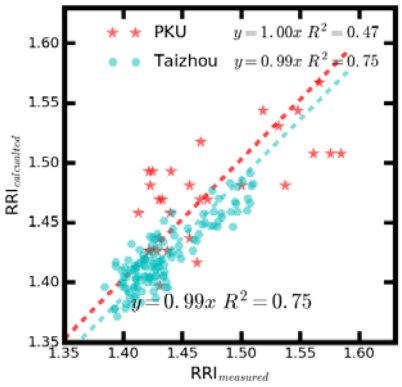

Fig. R1. Comparison between the measured and calculated RRI at PKU and Taizhou.

Comment: Also, an introduction how to use the parameterization in numerical models, i.e., what is the input and required parameters, may be required.

Reply: Our parameterization scheme is simple and easily used in numerical models because the effective density is the only parameter as input. We have demonstrated that the traditional method of calculating the RRI using aerosol main chemical components can have significant bias because the effects of organic aerosol is not considered. We added some discussions in the manuscript correspondingly.

Comment: Second, the main conclusion can be led from Figure 4. However, Figure 4 only indicates that Equation (1) is applicable for the effective particle (I understand this is also one of the findings in this study). I expect the clear evidence of the relationship between measured-RRI and calculated-RRI, as shown in Figures S8 and S9.

Reply: Thanks for the comment. We have replotted the figure 4.

Comment: Finally, in the result and discussion of section 3.4, the authors estimated the ARF, but the objectives of this section may be side tracked. Here, the authors

should discuss the impact of the parameterization on the ARF, but the conclusion is "the real-time measured RRI be used rather than a constant RRI when estimating the ambient aerosol optical and radiative properties". This conclusion confuses me. When the proposed parameterization is applied to numerical models, is the real-time measured RRI still required? If so, this parameterization is not attractive to modelers. In addition, the experimental conditions of the ARF calculation is unclear (see the below comment).

Reply: Thanks for the comments. Traditionally, a constant RRI is used when estimating the DARF. As shown in section 3.4, large uncertainties may arise when estimating the DARF using a constant RRI. The real time measured RRI should be used rather than a constant RRI in order to estimate the ambient aerosol optical and radiative properties with high accuracy. However, the real-time measurement of ambient aerosol RRI is not available for most of the conditions. Our proposed parameterization scheme can act as a substitute for real-time RRI.

We added some descriptions of method for ARF calculation in section S3 in the supplementary material.

Comment: In overall, the manuscript would be acceptable for publication if these comments can be satisfactorily addressed.

Reply: Thanks for the comment.

Comment: Specific comments: L23 (and L233): Only correlation coefficient is not enough to evaluate the relation. Please add the other statistical metrics.

Reply: Thanks for the comment. We have added the slope in the manuscript.

Comment: In abstract, the correlation coefficient is 0.75, but the value is 0.76 in Figure 4. Which is right?

Reply: Thanks for the comment. This is a typo and we corrected it.

Comment: L36: Which wavelengths are used?

Reply: Thanks for the comment. The wavelength range between 0.2 and 5 um is used for calculating the radiative forcing (Marshall et al., 1995; Moise et al., 2015). We have added the description in the text.

Comment: L103: Zhao et al. (2018b) seems to be still under discussion. The readers cannot trust the method only from the explanation in this manuscript.

Reply: Thanks for the comment. We added some discussions about this method in the manuscript. Before the measurement, this system is calibrated with ammonia sulfate (RRI=1.52). After calibration, ammonium chloride is used to validate the method of deriving the RRI from SP2 for different aerosol diameters. The RRI value of ammonium chloride is 1.642 (Lide, 2006). The retrieved RRI of ammonium chloride is in the range between 1.624 and 1.656. Therefore, this measurement system can measure the ambient aerosol RRI with high accuracy.

Comment: L144-145: RI of BC is set at 1.8+0.54i. Do the authors consider a dependence of RI on wavelength?

Reply: Thanks for the comment. The RI value of 1.8+0.54i is frequently used in estimating the radiative effects of BC particles (Bond et al., 2013; Zhao et al., 2018). The dependence of RI on wavelength for BC particle is not well studied yet (Bond and Bergstrom, 2006). Therefore, a constant RI of BC at different wavelength is used in estimating the DARF.

Comment: L159: Please clarify “parameterization aerosol vertical distributions”. This information is very important to estimate the ARF.

Reply: Thanks for the comment. We have added some descriptions in the section 3 of the supplementary material to introduce the method of calculating the aerosol vertical profiles.

Comment: L198-200: The RRI was measured at three different wavelengths (200nm, 300nm and 450nm). Here the measured RR is expressed as "1.34-1.56". Can the measured RRI at different wavelengths be combined? Do the authors consider the difference of RRI among the different wavelengths? In addition, is the focusing wavelength consistent to those proposed by the previous studies?

Reply: Thanks for the comment. The light scattering is measured by SP2 at the wavelength of 1064 and the measured RRI corresponds to the wavelength of 1064 nm. This system is no capable of measuring the RRI among different wavelengths. However, the measured RRI of ambient inorganic aerosols has little variation among different wavelengths. The RRI for $(NH_4)_2SO_4$ varies by 0.02 and less than 0.01 for wavelengths between 400 nm and 700 nm (Cotterell et al., 2017).

We conducted optical closure studies to demonstrate that the measured RRI at 1064 nm is applicable at other wavelength. First, the scattering coefficients (σ_{sca}) at wavelengths of 450, 525 and 635 nm were calculated using the measured refractive index at 1064 nm and Mie model (Bohren and Huffman, 2007) using the measured aerosol particle number size distribution and the BC mixing states. Then the calculated σ_{sca} are compared with the measured σ_{sca} by an nephelometer (Aurora 3000, Ecotech, Australia) (Müller et al., 2011). The Aurora 3000 is capable of measuring the σ_{sca} at 450, 525 and 635 nm. The scattering truncation and non-Lambertian error was corrected using the same method as that of Ma et al. (2011). The comparison of measured and calculated σ_{sca} are shown in fig. R2. The measured and calculated σ_{sca} show good consistence, demonstrating the measured RRI using our measurement system is applicable in other wavelength.

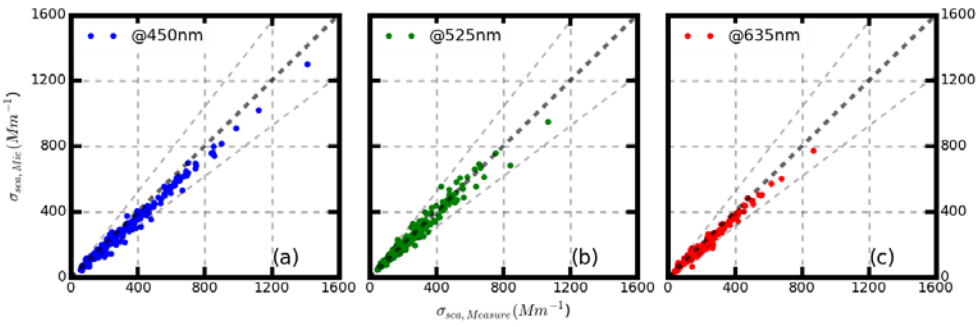

Figure R2. Comparison between the measured scattering coefficient and calculated scattering coefficient at (a) 450 nm, (b) 525 nm and (c) 635 nm.

Comment: L204-205: Can the authors explain the mechanism of the relationship between effective density and particle size?

Reply: Thanks for the comment. The difference of the effective density among different particle size should be resulted from the different chemical compositions. Based on the previous measurements of the size-resolved chemical compositions using a MOUDI, the mass fraction of OM decreases with the increment of aerosol diameter (Hu et al., 2012). At the same time, the effective density of OM is lower than the other inorganic compositions. Thus, the effective density increases with the increment of aerosol diameter.

Comment: Figure 5: Is the instant value or mean? Which wavelength do the authors calculate? Please clarify them.

Reply: Thanks for the comment. The calculated DARF from SBDARF is an instant value. The instant DARF is calculated over the wavelength range between 0.25 μm and 4 μm. We have added the descriptions in the text.

Comment: Figure S8 and S9: They are very interesting. I strongly recommend they are moved to the main text. Can the authors show the same figures estimated from the current study?

Reply: Thanks for the comment. Fig. 4 is replotted. Fig. S8 and fig. S9 were merged into figure 5.

Comment: Technical comments" L34: prat –> part

Reply: Thanks for the comment. We have revised it.

Comment: L46: It is better to add “n: refractive index” to the explanation of Equation (1).

Reply: Thanks for the comment. We have changed the equation as

$$RRI_{eff} = \sum_{i} (f_i \cdot RRI_i)$$

Where f_i and RRI_i are the volume fraction and real part of refractive index of known composition *i*.

Comment: L52: ne –> neff is suitable.

Reply: Thanks for the comment. We changed the "n" into RRI_{eff} in the manuscript.

Comment: Figure S1 (a), S4, S5: Better to be moved to the main text.

Reply: Thanks for the comment. Fig. S1 is moved into Fig. 2 in the text and part of fig. S4 is moved to the main text.

Bohren, C.F., Huffman, D.R., (2007) Absorption and Scattering by a Sphere, Absorption and Scattering of Light by Small Particles. Wiley-VCH Verlag GmbH, pp. 82-129.

Bond, T.C., Bergstrom, R.W. (2006) Light Absorption by Carbonaceous Particles: An Investigative Review. Aerosol Science And Technology 40, 27-67.

Bond, T.C., Doherty, S.J., Fahey, D.W., Forster, P.M., Berntsen, T., DeAngelo, B.J., Flanner, M.G., Ghan, S., Karcher, B., Koch, D., Kinne, S., Kondo, Y., Quinn, P.K., Sarofim, M.C., Schultz, M.G., Schulz, M., Venkataraman, C., Zhang, H., Zhang, S., Bellouin, N., Guttikunda, S.K., Hopke, P.K., Jacobson, M.Z., Kaiser, J.W., Klimont, Z., Lohmann, U., Schwarz, J.P., Shindell, D., Storelvmo, T., Warren, S.G., Zender, C.S. (2013) Bounding the role of black carbon in the climate system: A scientific assessment. Journal Of Geophysical Research-Atmospheres 118, 5380-5552.

Cotterell, M.I., Willoughby, R.E., Bzdek, B.R., Orr-Ewing, A.J., Reid, J.P. (2017) A complete parameterisation of the relative humidity and wavelength dependence of the refractive index of hygroscopic inorganic aerosol particles. Atmospheric Chemistry and Physics 17, 9837-9851.

Han, Y., Lü, D., Rao, R., Wang, Y. (2009) Determination of the complex refractive indices of aerosol from aerodynamic particle size spectrometer and integrating nephelometer measurements. Applied Optics 48, 4108-4117.

Hu, M., Peng, J., Sun, K., Yue, D., Guo, S., Wiedensohler, A., Wu, Z. (2012) Estimation of size-resolved ambient particle density based on the measurement of aerosol number, mass, and chemical size distributions in the winter in Beijing. Environ Sci Technol 46, 9941-9947.

Lide, D.R. (2006) Handbook of Chemistry and Physics, 86th Edition Edited(National Institute of Standards and Technology). Journal of the American Chemical Society 128, 5585-5585.

Ma, N., Zhao, C.S., Nowak, A., Müller, T., Pfeifer, S., Cheng, Y.F., Deng, Z.Z., Liu, P.F., Xu, W.Y., Ran, L., Yan, P., Göbel, T., Hallbauer, E., Mildenberger, K., Henning, S., Yu, J., Chen, L.L., Zhou, X.J., Stratmann, F., Wiedensohler, A. (2011) Aerosol optical properties in the North China Plain during HaChi campaign: an in-situ optical closure study. Atmos. Chem. Phys. 11, 5959-5973.

Marshall, S.F., Covert, D.S., Charlson, R.J. (1995) Relationship between asymmetry parameter and hemispheric backscatter ratio: implications for climate forcing by aerosols. Applied Optics 34, 6306-6311.

Moise, T., Flores, J.M., Rudich, Y. (2015) Optical properties of secondary organic aerosols and their changes by chemical processes. Chemical Reviews 115, 4400-4439.

Müller, T., Laborde, M., Kassell, G., Wiedensohler, A. (2011) Design and performance of a three-wavelength LED-based total scatter and backscatter integrating nephelometer. Atmos. Meas. Tech. 4, 1291-1303.

Zhao, G., Zhao, C., Kuang, Y., Bian, Y., Tao, J., Shen, C., Yu, Y. (2018) Calculating the aerosol asymmetry factor based on measurements from the humidified nephelometer system. Atmospheric Chemistry and Physics 18, 9049-9060.

A new parameterization scheme of the real part of the ambient aerosols refractive index

Gang Zhao[1], Tianyi Tan[2], Weilun Zhao[1], Song Guo[2], Ping Tian[3], Chunsheng Zhao[1*]

1 Department of Atmospheric and Oceanic Sciences, School of Physics, Peking University, Beijing, China

2 State Key Joint Laboratory of Environmental Simulation and Pollution Control, College of Environmental Sciences and Engineering, Peking University, Beijing 100871, China

3 Beijing Key Laboratory of Cloud, Precipitation and Atmospheric Water Resources, Beijing 100089, China

[*]**Correspondence to: Chunsheng Zhao (zcs@pku.edu.cn)**

Abstract

The refractive index of ambient aerosols, which directly determines the aerosol optical properties, is widely used in atmospheric models and remote sensing. Traditionally, the real part of the refractive index (RRI) is mainly parameterized by the measurement of ambient aerosol main inorganic components. In this paper, the characteristics of the ambient aerosol RRI are studied based on the field measurement in the East China. Results show that the ambient aerosol RRI varies significantly between 1.36 and 1.56. The direct aerosol radiative forcing is estimated to vary by 40% corresponding to the variation of the measured aerosol RRI. We find that the ambient aerosol RRI is highly related with the aerosol effective density (ρ_{eff}) rather than the main chemical components. However, parameterization schemes of the ambient aerosol RRI by ρ_{eff} are not available due to the lack of corresponding simultaneous field measurements. For the first time, the size-resolved ambient aerosol RRI and ρ_{eff}

are measured simultaneously by our designed measurement system. A new parameterization scheme of the ambient aerosols RRI using ρ_{eff} is proposed. The measured and parameterized RRI agree well with the correlation coefficient of 0.~~76~~75 and slope of 0.99. Knowledge of the ambient aerosol RRI would improve our understanding of the ambient aerosol radiative effects.

1 Introduction

Atmospheric aerosols can significantly influence the ~~reginal~~ regional air quality and climate system by scattering and absorbing the solar radiation (Seinfeld et al., 1998). However, estimation of the aerosol radiative effects remains large uncertainties due to the high temporal and spatial variations in aerosol microphysical properties (Levoni et al., 1997). The complex refractive index (RI), which directly determines the aerosol scattering and absorbing abilities (Bohren and Huffman, 2007), is one of the most important microphysical parameters of aerosol optics and radiation. RI is widely employed in atmospheric models and remote sensing (Zhao et al., 2017). When estimating the direct aerosol radiative forcing (DARF), many studies showed that great uncertainties may arise due to small uncertainties in the real ~~prat~~ part of the RI (RRI). ~~For non-absorbing particles, i~~It was found that a small perturbation in RRI (0.003) can lead to an uncertainty of 1% in DARF for non-absorbing particles (Zarzana et al., 2014). An increment of 12% in the DARF occurred when the RRI increase~~s~~d from 1.4 to 1.5 (Moise et al., 2015) over the wavelength range between 0.2 μm and 5 μm. Therefore, it is necessary to measure or parameterize the ambient aerosol RRI with high accuracy.

Traditionally, the RRI is ~~determined~~derived ~~by~~from measurements of aerosol main inorganic chemical compo~~nents~~sitions (Han et al., 2009). For the ambient aerosol with multiple components, ~~a common approach to calculate the aerosol effective RRI by~~ linear volume average of known aerosol chemical composition is widely used to estimate the aerosol effective RRI_{eff} (Hand and Kreidenweis, 2002;Liu and Daum, 2008;Hänel, 1968;Wex et al., 2002) with ~~:, which calculates the RRI by integrating partial refractive index n_i weighted with the volume fraction f_i:~~

$$RRI_{eff}~~n_e~~ = \sum_i (f_i~~n~~ \cdot RRI_i) \qquad (~~2~~1)$$

Where f_i and RRI_i are the volume fraction and real part of refractive index of known composition *i*. However, the influences of organic component on the aerosol RRI were not considered when estimating the RRI using the traditional method. The organic component contributes more than 20% of the total aerosol component in China (Hu et al., 2012;Liu et al., 2014). At the same time, RRI of the organic aerosol changes significantly between 1.36 and 1.66 (Moise et al., 2015). Ignoring the organic component may lead to significant biases when estimating the ambient aerosol RRI. The comparison between the estimated RRI using main aerosol main aerosol composition and measured aerosol RRI using other method was not available due to the lack of measurement of ambient aerosol RRI.

Information of RRI may be helpful for the knowledge of ambient aerosol chemical information. ~~Up until now, there is limit information about the size-resolved RRI ($\widetilde{RRI}$) of ambient particles. However,~~ ~~m~~Many studies find that ambient aerosols of different size have different properties such as shape (Peng et al., 2016), chemical composition (Hu et al., 2012) and density (Qiao et al., 2018). Up until now, there is limit information about the size-resolved RRI ($\widetilde{RRI}$) of ambient particles. Characteristics of the ambient aerosol $\widetilde{RRI}$ were not well studied yet.

The RRI of mono-component particle is defined ~~by~~as (Liu and Daum, 2008):

$$\frac{\text{~~n~~}RRI^2-1}{\text{~~n~~}RRI^2+2}=\frac{N_A\alpha}{3M}\rho_{eff} \qquad (\text{~~1~~}2)\text{~~,~~}$$

where N_A is the universal Avagadro's number, α is the mean molecular polarizability, M is the molecular weight of the material and ρ_{eff} is the mass effective density of the chemical component. The RRI should be highly related to ρ_{eff}. However, there was no study that investigated the relationship between the RRI and ρ_{eff} of ambient aerosol.

The ρ_{eff} of ambient aerosols is one of the crucial parameters in aerosol thermo-dynamical and optical models. ~~The ρ_{eff}~~It can ~~also~~ be used to infer the ambient particle aging process (Peng et al., 2016). Based on equation ~~1~~2, the aerosol ρ_{eff} is directly related to the aerosol RRI. Few studies measure the ambient aerosol RRI and ρ_{eff} simultaneously. So far, parameterizations of the RRI by ρ_{eff} using the simultaneous measurements are not available. Real-time measurements of the ~~size-resolved~~ ρ_{eff} ~~($\widetilde{\rho_{eff}}$) combined with~~and ~~the~~ aerosol RRI~~$\widetilde{RRI}$~~ concurrently can help to better understand the relationship between the aerosol RRI and ρ_{eff}.

In this study, the aerosol $\widetilde{RRI}$ and size resolved ρ_{eff} ($\widetilde{\rho_{eff}}$) are measured simultaneously during a field measurerument conducted in Taizhou in the East China. The ambient aerosol $\widetilde{RRI}$ is measured by our designed system, which combines a differential mobility analyzer (DMA) and a single particle soot photometer (SP2) (Zhao et al., 2018b). The $\widetilde{\rho_{eff}}$ is measured by using a centrifugal particle mass analyzer (CMPA) and a scanning mobility particle sizer (SMPS). The characteristic of the $\widetilde{RRI}$ and $\widetilde{\rho_{eff}}$ are analyzed in this study. It is the first time that the $\widetilde{RRI}$ and $\widetilde{\rho_{eff}}$ of the ambient aerosol are measured simultaneously. For the first time, aA parameterization scheme of the RRI by the ρ_{eff} using the simultaneous measurement is proposed. Based on the measured variability of the measured RRI, we estimated the corresponding variation of the aerosol direct aerosol radiative forcing, which to some extent give valuable knowledge for the influence of aerosol RRI variations on aerosol radiative effects.

The structure of this study is as follows: the descriptions of the instrument setup is given in section 2.1, 2.2 and 2.3. The methodology of evaluating the aerosol optical properties and radiative effects corresponding to the variations of the measured RRI isare shown in section 2.4 and 2.5 respectively. Section 3.1 describes the characteristics of the measured the $\widetilde{RRI}$ and $\widetilde{\rho_{eff}}$. Section 3.3 proposes the parameterization of the aerosol RRI. The corresponding variations in aerosol optical properties and radiative effects corresponding to the variations of the measured RRI are both discussed in section 3.4.

2 Data and Methods

2.1 Description of the measurement campaign

The measurement was conducted in a suburban site Taizhou (119°57'E, 32°35'N), as shown in fig. 1(a), which lies in the south end of the Jianghuai Plain in the central Eastern China. It is located on the north east of the megacity Nanjing with a distance of 118 km. Another megacity Shanghai is 200 km away from Taizhou in the southeastern direction. The industrial area between Nanjing and Shanghai has experienced severe pollutions in the past twenty years. The average Moderate Resolution Imaging Spectroradiometer (MODIS) aerosol optical depth data at 550nm over the year 2017, as shown in fig. 1(b), also reflects that the measurement site is more polluted than the surrounding areas.

During the field campaign, all of the instruments were placed in a container, in which the temperature was well controlled within 24±2 °C. The sample air was collected from a PM_{10} impactor (Mesa Labs,

Model SSI2.5) mounted on the top of the container and then passed through a Nafion dryer tube to ensure that the relative humidity of the sample particles was controlled below 30%.

Along with the measurement of the $\widetilde{RRI}$ and $\widetilde{\rho_{eff}}$, the aerosol scattering coefficients (σ_{sca}) at three different wavelengths (450, 525 and 635 nm) were measured by an nephelometer (Aurora 3000, Ecotech, Australia) (Müller et al., 2011) at a resolution of 5 minutes. The scattering truncation and non-Lambertian error was corrected using the same method ~~in~~ as that of Ma et al. (2011). ~~The mass concentration of the black carbon (m_{BC}) is measured by an aethalometer (AE33) (Drinovec et al., 2015) and the σ_{abs} is recorded every minute.~~ The aerosol water-soluble ions (NH_4^+, SO_4^{2-}, NO_3^-, Cl^-) of $PM_{2.5}$ were measured by an In situ Gas and Aerosol Compositions Monitor (TH-GAC3000, China). The mass concentration of elementary carbon and organic carbon (OC) were measured using a thermal optical transmittance aerosol carbon analyzer (ECOC, Focused Photonics Inc.). The concentrations of Organic matters (OM) are achieved through multiplying OC concentration by 1.4 (Hu et al., 2012). The time resolution of the aerosol composition measurement was one hour.

~~An automatic weather station was located next to the aerosol measurement container. The wind speed, wind direction, temperature (T) and relative humidity (RH) were measured in 1-minute time resolution.~~

2.2 Measuring the $\widetilde{RRI}$

A coupling DMA-SP2 system was employed to measure the aerosol $\widetilde{RRI}$ from 24th, May to 18th, June in 2018. This system is introduced elsewhere by Zhao et al. (2018b) and a brief description is presented here. As schematically shown in fig. S1, the monodispersed aerosols selected by a DMA (Model 3081, TSI, USA) are drawn into a SP2 to measure the corresponding scattering properties. The SP2 is capable of distinguishing the pure scattering aerosols from the black carbon (BC) containing aerosols by measuring the incandescence signals at 1064 nm. For the pure scattering aerosol, the scattering strength (S) measured by SP2 is expressed as:

$$S = C \cdot I_0 \cdot (\sigma_{45^o} + \sigma_{135^o}) \qquad (3),$$

where C is a constant that is determined by the instrument response character; I_0 is the instrument's laser intensity; σ_{45^o} and σ_{135^o} is the scattering function of the sampled aerosol at 45° and 135°, respectively;. From Mie scattering theory–, aerosol size and RRI directly determine the scattering function at a given direction. Inversely, the aerosol RRI can be retrieved when the aerosol size and scattering strength are determined. This system can measure the– ambient aerosol $\widetilde{RRI}$ with uncertainty less than 0.02 (Zhao et al., 2018b).

Before the measurement, this system is calibrated with ammonia sulfate (RRI=1.52). The relationships between the diameter and the measured scattering peak height are shown in fig. S2. After calibration, ammonium chloride is used to validate the method of deriving the RRI at different aerosol diameters. The RRI value of ammonium chloride is 1.642 (Lide, 2006) and the measured RRI of ammonium chloride is in the range between 1.624 and 1.656 in our study. Therefore, this measurement system can measure the ambient aerosol RRI with high accuracy.

2.3 Measuring the $\widetilde{\rho_{eff}}$

The $\widetilde{\rho_{eff}}$ is measured by a Centrifugal Particle Mass Analyzer (CPMA, version 1.53, Cambustion Ltd, UK) in tandem with a Scanning Mobility Particle Sizer (SMPS) system from 12th, June to 18th, June in 2018. The ρ_{eff} is defined as

$$\rho_{eff} = \frac{m_p}{\frac{\pi}{6} \times d_m^3} \qquad (4),$$

Where m_p is the particle mass and d_m is the aerosol mobility diameter selected by DMA.

The controlling of the CPMA-SMPS system is achieved by self-established Labview software. The CPMA is set to scan twelve different aerosol mass at 1.0, 1.4, 2.0, 2.9, 4.2, 5.9, 8.5, 12.1, 17.2, 24.6, 35.0 and 50.0 fg every five minutes respectively. The SMPS scan the aerosol diameters between 60nm and 500nm every 5 minute, which results in a period of one hour for measuring the effective density of different mass.

At the beginning of the field measurement, the CPMA-SMPS system is calibrated using the PSL particles with different mass. The corresponding measured effective densities of PSL particles are 1.04 and 1.07 g/cm^3, which agree well with the PSL material density of 1.05 g/cm^3.

2.4 Calculate aerosol optical properties using different RRI

The aerosol optical properties are highly related to the RRI. From Mie scattering theory, the variation in aerosol RRI may result in significant variations in the aerosol optical properties, such as aerosol extinction coefficient (σ_{ext}), the σ_{sca}, the single scattering albedo (SSA), and the asymmetry factor (g) (Bohren and Huffman, 2007). SSA is defined as the ratio of σ_{sca} to σ_{ext}, which reflects concentration of the absorbing aerosol (Tao et al., 2014) to some extent. The g expresses the distribution of the scattering light intensity in different directions (Zhao et al., 2018a). The σ_{ext}, SSA and g are the most important three factors that influence the aerosol radiative properties in radiative calculation (Kuang et al., 2015).

In this study, the sensitivity studies of the aeorsol optical proprties to the aerosol RRI are carried out by employing the Mie scattering theory. The input variables of Mie scattering model includes the aerosol PNSD and BC mixing state and aerosol complex refractive index. The Mie model can calculate the σ_{ext}, σ_{sca}, SSA and g. The mixing state of the ambient BC comes from the measurements of the DMA-SP2 system. All of the aerosols are divided into pure scattering aerosols and BC-containing aerosols. The BC-containing aerosols are assumed to be core-shell mixed. As for the RI of BC, 1.8+0.54i is used (Kuang et al., 2015). With this, the aerosol σ_{ext}, σ_{sca}, SSA and g at different RRI values can be calculated.

2.5 Estimating the aerosol DARF

In this study, the DARF under different aerosol RRI conditions is estimated by the Santa Barbara DISORT (discrete ordinates radiative transfer) Atmospheric Radiative Transfer (SBDART) model (Ricchiazzi et al., 1998). Under the cloud-free conditions, DARF at the TOA is ~~defined~~ calculated as the difference between radiative flux under aerosol-free conditions and aerosol present conditions:

$$DARF = (f_a\downarrow - f_a\uparrow) - (f_n\downarrow - f_n\uparrow) \quad (5),$$

where $f_a\downarrow$ and $f_a\uparrow$ are the downward and upward radiative irradiance with aerosol present conditions respectively; the difference between $f_a\downarrow$ and $f_a\uparrow$ $(f_a\downarrow - f_a\uparrow)$ is the downward radiative irradiance flux with aerosol present conditions; $f_n\downarrow$ and $f_n\uparrow$ correspond to the downward and upward radiative irradiance values under aerosol free conditions respectively; the difference between $f_n\downarrow$ and $f_n\uparrow$ $(f_n\downarrow - f_n\uparrow)$ is the downward radiative irradiance flux for aerosol-free conditions

(Kuang et al., 2016). The instant DARF value is calculated over the wavelength range between 0.25 μm and 4 μm.

Input data for the model are shown below. The vertical profiles of temperature, pressure and water vapor, which ~~are the mean results of~~adopt the radiosonde observations at Taizhou site ~~during the field measurement~~. The measured mean results corresponding the field measurement period are used. Vertical distributions of aerosol σ_{ext}, SSA and g with a resolution of 50 m, are resulted from the calculation using the Mie Model and parameterized aerosol vertical distributions. Methods for parameterization and calculation of the aerosol optical profiles can be found in Sect. S3 or in ~~More details of calculating the optical profiles can refer to~~ Zhao et al. (2018a). The surface albedo adopt the mean results of MODIS V005 Climate Modeling Grid (CMG) Albedo Product (MCD43C3) at the area of Taizhou from May, 2017 to April, 2018. The other default values are used in the simulation (Ricchiazzi et al., 1998).

3 Results and Discussions

3.1 The Measurements Results

The overview of the measurement is shown in fig. 2~~S4~~. During the measurement, ~~the mean wind speed is relatively low with 2.13±1.13 m/s. The prevailing speed is south wind and south east wind. The average T and RH are 23±6.4°C and 74.0±18.7% respectively. The T and RH show evident diurnal cycles as illustrated in fig. S5 (a) and (b). The T gets its peak values at 15:00 in the afternoon and the lowest value at 4:00 at night. The RH exhibited opposite trend. During the campaign, the rain occurred at the night of 25th, 28th, 31st in May, which can be reflected by the high RH shown in fig. S4 (b). The mean m_{BC} is 3.82±3.37 μg/m^3 and the mean σ_{sca} at 525 nm is 276±230 Mm^{-1}. Both the m_{BC} and σ_{sca} shows evident diurnal variation based on fig. S5 (c) and (d), which is highly related to the development of the mixing layer height, the local emission and the ambient aging process. The m_{BC} and σ_{sca} peak at around 7:00 in the morning and reach the valley at 15:00 in the afternoon. The peak values of the m_{BC} and σ_{sca} are about three time of the minimum value correspondingly.~~

~~Based on the m_{BC} and σ_{sca} time series,~~ the σ_{sca} is relatively low with a mean value of 167±74 Mm^{-1}. T~~t~~here were ~~total two~~ one major pollution episodes occurred based on the σ_{sca} time series ~~during this campaign~~ as shown in fig. 2(a). This ~~e first episode happens from 28th, May to 30th, May~~

~~and the maximum values of m_{BC} and σ_{sca} reach 20 μg/m^3 and 1197 Mm^{-1}, which is about 5 times the concentrations of the mean aerosol loading. The second period of~~ pollution happens ~~from the night of 4~~on 13th, June ~~to 7th June,~~ and doesn't last long. The corresponding ~~m_{BC} and~~ σ_{sca} reaches ~~14 μg/m^3 and 1210~~540 Mm^{-1}. A moderate polluted condition between 14~~1~~~~th~~st, June and ~~3~~~~rd~~15th, June is observed. ~~Another moderate pollution happens during the 11th, June and 14th, when the $\widetilde{RRI}$ and $\widetilde{\rho_{eff}}$ are measured simultaneously.~~ The aerosol PNSD changes substantially with the pollution conditions as shown in fig. 2(b). The geometric median aerosol diameter changes between 30 nm and 105 nm. The median diameter tends to be lower when the surrounding is cleaner. Despite the median diameter reaches 105 nm on 16th, June, the surrounding is relative clean due to the low aerosol number concentration.

~~Fig. 1 shows the time series of the concurrently measured $\widetilde{RRI}$ and $\widetilde{\rho_{eff}}$. During this period, the σ_{sca} is relatively low with a mean value of 167±74 Mm^{-1}.~~ The $\widetilde{RRI}$ and $\widetilde{\rho_{eff}}$ vary from 1.34 to 1.54 and the $\widetilde{\rho_{eff}}$ ranges between 1.21 to 1.80 g/cm^3 as shown in fig. 2 (c) and (d). From fig. ~~1~~2, the measured RRI shows the same variation pattern with the ρ_{eff}. Both the $\widetilde{RRI}$ and $\widetilde{\rho_{eff}}$ increase with the diameter, which may indicate that the aerosol chemical composition varies among different aerosol particle size.

As for the $\widetilde{RRI}$, ~~the measured RRI values of ambient aerosol for 200nm, 300nm and 450nm show large variations from 1.36 to 1.56. The~~ the corresponding mean RRI values for aerosol diameter at 200nm, 300nm and 450nm are 1.425±0.031, 1.435±0.041, 1.47±0.059 ~~as shown in fig. S4 (e)~~. When comparing the probability distribution of the RRI for different diameter in fig. 3 ~~3 (b), (d) and (f)~~, ~~we find that~~ the RRI is more dispersed when the particle size increases, implicating that the aerosol compositions become complicated when the aerosol get aged. Fig. ~~3~~ 3 (a), (c) and (e) give diurnal variation of the $\widetilde{RRI}$ values at different particle sizes of 200 nm, 300 nm and 450 nm. The RRI shows ~~slightly~~ diurnal cycles for different diameters. They reach the peak at about 15:00 in the morning and fall to the valley at around 9:00 in the afternoon.

The range of the measured RRI (1.34~1.56) is a little ~~larger~~ wider than the literature values. The past measurement of the ambient aerosol RRI values varies between 1.4 and 1.6 (Dubovik, 2002;Guyon et

al., 2003;Zhang et al., 2016) over different measurement site. This is the first time that such high variations in ambient aerosol RRI were observed at one site.

The $\widetilde{\rho_{eff}}$ shows almost the same diurnal variations as the $\widetilde{RRI}$ as shown fig. ~~S6~~S5. The diurnal variations of the $\widetilde{\rho_{eff}}$ is more dispersed because the time period of measuring the $\widetilde{\rho_{eff}}$ is shorter (7 days) comparing with the time of $\widetilde{RRI}$ (28 days). It is evident that the ρ_{eff} increased with particle size. The difference of ρ_{eff} among different particle size should be resulted from different contributions of chemical compositions, especially the OM. Based on the previous measurement of the size-resolved chemical compositions using a micro orifice uniform deposit impactors (MOUDI), the mass fraction of OM get decreased with the increment of aerosol diameter (Hu et al., 2012). At the same time, the effective density of OM is lower than the other main inorganic compositions. Thus, the effective tend to increase with the increment of aerosol diameter.

3.2 Aerosol Chemical Composition versus the RRI

From equation (1) and (2), the aerosol RRI can be determined by aerosol chemical composition (Liu and Daum, 2008). Many studies calculate the RRI using the measurement results of the relative contributions of aerosol chemical composition (Yue et al., 1994;Hänel, 1968;Guyon et al., 2003;Stelson, 1990;Wex et al., 2002). However, there is no comparison between the RRI calculated from chemical composition and real-time measurement until now. In this study, the relationship between the measured RRI and the mass fraction of each ion components is investigated.

As illustrated in fig. ~~3~~4, the RRI tend to increase with the OM mass fraction ratio, which implies that the OM may play an important role in aerosol scattering properties. This is in agreement with the Aldhaif et al. (2018), where the aerosol OM contributes a lot to the ambient aerosol mass concentrations. The RRI have implicit relationship with the mass fraction of the σ_{sca} at 525 nm, SO_4^{2-}, Cl^-, and NO_3^-. The mass ratio of NH_4^+ seems to be negatively correlated with the RRI. At the same time, the measured RRI values have no clear relationship with the absolute mass concentrations of the main aerosol chemical components, as shown in fig. ~~S7~~S6.

The RRI is also calculated by applying the method proposed by Stelson (1990), in which the bulk chemical composition is used. The comparison between the calculated RRI and the measured RRI is shown in fig. ~~S8~~5. It can be noticed that the calculated RRI and the measured RRI doesn't agree well.

There are several reasons that may cause the discrepancies. The first reason might be that the aerosol chemical information used in the method is the average mass of whole aerosol population. The aerosol chemical composition may vary significantly among different size. Secondly, the OM of the ambient aerosols is very complicated and the influence of the OM on the aerosol RRI has not been studied well. Therefore, more research is necessary when parameterizing the ambient aerosol RRI with the measured aerosol chemical composition.

3.3 Parameterizing the RRI using ρ_{eff}

As shown in fig. ~~1~~2, there is good consistence between the variation of the measured $\widetilde{RRI}$ and $\widetilde{\rho_{eff}}$. When defining the specific refractive index Re with $Re = \frac{n RRI^2-1}{n RRI^2+2}$, we found that the Re is highly correlated with ρ_{eff} by a R^2 equaling 0.7~~5~~6 and slope 0.99 (fig. ~~4~~5). The linear relationships between the Re and ρ_{eff} is:

$$\frac{RRI^2-1}{RRI^2+2} = 0.18\rho_{eff} \qquad (6~~5~~).$$

The RRI can be calculated based on equation 6:

$$RRI = \sqrt{\frac{1+0.36\rho_{eff}}{1-0.18\rho_{eff}}} \qquad (7).$$

Based on equation 7~~(5)~~ and fig. ~~4~~ 6 the aerosol RRI can be parameterized by the ρ_{eff} with high accuracy and the uncertainties of the calculated RRI using equation 7~~5~~ can be constrained within 0.025. The aerosol ρ_{eff} is easier to be measured, and equation ~~5~~ 7 might be used as a good probe of parameterizing the RRI.

To demonstrate the universality of this parameterization scheme, we conducted another measurement in the campus of Peking University (PKU) (N39°59′, E116°18′), in North China Plain, where the aerosol effective density and real part of the refractive index are measured concurrently at 16th, December in 2018. The measurement last only one days because some instruments were borrowed from other institute. The RRI were also calculated using the parameterization scheme equation 7. The slope and correlation coefficient at PKU site are 1.0 and 0.47 respectively. The calculated and measured RRI show good consistence. Therefore, this scheme is applicable for different seasons at both Center China and North China Plain.

This parameterization scheme is easy to use because the effective density is the only parameter used as input. We have demonstrated that the traditional method of calculating the RRI using aerosol main chemical components can have significant bias because the effects of organic aerosol is not considered. The RRI can be easy to calculate based on our parameterization scheme, as the effective density of ambient aerosol is rather easier to measure.

In the previous, Liu and Daum (2008) summarized some of the measured RRI and the ρ_{eff}, and parameterized the RRI as

$$\frac{\text{~~n~~RRI}^2-1}{\text{~~n~~RRI}^2+2} = 0.23\rho^{0.39} \qquad (\text{~~8~~6}).$$

The feasibility of this scheme is tested here and the results are shown in fig. ~~S9~~5. The measured and parameterized RRI using the method of Liu and Daum (2008) deviated from 1:1 line. The effective density and RRI in their work were estimated using the aerosol chemical components but not the field measurement. At the same time, the influence of organic aerosols components on aerosol RRI is not considered in their work.~~The deviations might be caused by that the proposed parameterization scheme by Liu and Daum (2008) does not base on the simultaneous field measurement.~~

3.4 Influence of RRI Variation on Aerosol Optical Properties and Radiative Properties

The measured RRI varies between 1.34 and 1.56 during the field campaign. The corresponding aerosol optical properties are estimated. When estimating the aerosol optical properties with different aerosol RRI, the measured mean aerosol PNSD and mixing states are used. Fig. ~~5~~ 7 gives the variation of the aerosol σ_{sca}, SSA and g. From fig. ~~5~~7, the σ_{sca} varies from 162 Mm^{-1} to 308 Mm^{-1}. The SSA varies between 0.843 and 0.895, which matches the variations of the dry aerosol SSA for different aerosol size distributions in the North China Plain (NCP) (Tao et al., 2014). As for the aerosol g, it decreases from 0.667 to 0.602 with the increment of the aerosol RRI. The ambient g values in the NCP are found within 0.55 and 0.66 (Zhao et al., 2018a). Thus, the variations of the RRI have significant influence on the g. The aerosol optical properties change significantly with the variation of the ambient aerosol RRI.

The instant DARF values under different RRI are also estimated and the results are illustrated in fig. ~~5~~7(b). When the aerosol RRI increases from 1.4 to 1.5, the DARF varies from -6.17 to -8.35, corresponding to 15% variation in DARF. This values are in accordance with the work of Moise et al.

(2015), who estimate that an increment of 12% in the DARF occurs when the RRI varies from 1.4 to 1.5. The DARF can change from -4.9 w/m^2 to -10.14 w/m^2 when the aerosol RRI increase from 1.34 to 1.56, which corresponding to 40% variation in DARF. Great uncertainties may arise when estimating the aerosol radiative forcing when using a constant RRI. The RRI should be different under different aerosol conditions. The real time measured RRI should be used rather than a constant RRI when estimating the ambient aerosol optical and radiative properties. However, the real-time measurement of ambient aerosol RRI is not available for most of the conditions. Our proposed parameterizations scheme is a perfect substitute. The only parameter required is aerosol effective density and it is much easier to measure. ~~We recommend that the real-time measured RRI be used rather than a constant RRI when estimating the ambient aerosol optical and radiative properties.~~

4 Conclusions

The ambient aerosol RRI is a key parameter in determining the aerosol optical properties and knowledge of it can help constrain the uncertainties in aerosol radiative forcing. In this study, the ambient aerosol $\widetilde{RRI}$ were measured at Taizhou, in the Jianghuai Plain of China by using a DMA in tandem with a SP2 from 24th, May to 18th, June in 2018.

Results show that the ambient aerosol RRI varies over a wide range between 1.34 and 1.56. The RRI increases slowly with the increment of the aerosol diameter. The mean aerosol RRI values are 1.425±0.031, 1.435±0.041, 1.47±0.059 for aerosol diameter at 200_nm, 300_nm and 450_nm respectively. Probability distributions of the RRI show that the RRI is more dispersed with the increment of aerosol dimeter, which reflect the complexing aging processing of the ambient aerosol. The aerosol optical properties change significantly and the DARF is estimated to vary by 40% corresponding to the variation of the measured ambient aerosol RRI. The real-time measured RRI should be used rather than a constant RRI when estimating the ambient aerosol optical and radiative properties.

Traditionally, the ambient aerosol RRI is mainly calculated by using the corresponding measured main chemical inorganic compositions of aerosols. We find that the ambient aerosol RRI is highly related with the ρ_{eff} rather than the main chemical compositions of aerosols. There is discrepancy

between the measured and parameterized RRI using the traditional method. This might be resulted from two reasons. The first one is that the aerosol chemical information used for calculation is the total aerosol loading. The aerosol chemical compositions may change significantly among different size. Another one is that the influence of OM of ambient aerosols is not considered. The RRI of OM varies significantly for different compositions (Moise et al., 2015).

Despite that the RRI is related with the ρ_{eff}, parameterization scheme of the ambient aerosol RRI using ρ_{eff} is not available due to the lack of simultaneously measurement. For the first time, the $\widetilde{RRI}$ and $\widetilde{\rho_{eff}}$ were measured simultaneously using our designed system. The $\widetilde{\rho_{eff}}$ is measured during the field campaign by employing a CMPA and a SMPS from 12th, June to 18th, June in 2018.

A new parameterization scheme of the ambient aerosol RRI using the ρ_{eff} is proposed based on the field measurement results. The measured and parameterized RRI agree well with the correlation coefficient of 0.75 and slope of 0.996. This parameterization scheme is validated at another measurement site at different season. This simple scheme is reliable and ready to be used in the calculation of aerosol optical and radiative properties. The corresponding measurement results can also be further used in climate model.

Competing interests. The authors declare that they have no conflict of interest.

Data availability. The data used in this study is available when requesting the authors.

Author contributions. GZ, CZ, WZ and SG designed and conducted the experiments; PT, TY and GZ discussed the results.

Acknowledgments. This work is supported by the National Natural Science Foundation of China (41590872) and National Key R&D Program of China (2016YFC020000:Task 5).

References

Aldhaif, A. M., Stahl, C., Braun, R. A., Moghaddam, M. A., Shingler, T., Crosbie, E., Sawamura, P., Dadashazar, H., Ziemba, L., Jimenez, J. L., Campuzano-Jost, P., and Sorooshian, A.: Characterization

of the Real Part of Dry Aerosol Refractive Index Over North America From the Surface to 12 km, Journal of Geophysical Research: Atmospheres, 10.1029/2018jd028504, 2018.

Bohren, C. F., and Huffman, D. R.: Absorption and Scattering by a Sphere, in: Absorption and Scattering of Light by Small Particles, Wiley-VCH Verlag GmbH, 82-129, 2007.

Drinovec, L., Močnik, G., Zotter, P., Prévôt, A. S. H., Ruckstuhl, C., Coz, E., Rupakheti, M., Sciare, J., Müller, T., Wiedensohler, A., and Hansen, A. D. A.: The "dual-spot" Aethalometer: an improved measurement of aerosol black carbon with real-time loading compensation, Atmospheric Measurement Techniques, 8, 1965-1979, 10.5194/amt-8-1965-2015, 2015.

Dubovik, O.: Variability of absorption and optical properties of key aerosol types observed in worldwide locations, J.atmos.sci, 59, 590-608, 2002.

Guyon, P., Boucher, O., Graham, B., Beck, J., Mayol-Bracero, O. L., Roberts, G. C., Maenhaut, W., Artaxo, P., and Andreae, M. O.: Refractive index of aerosol particles over the Amazon tropical forest during LBA-EUSTACH 1999, Journal of Aerosol Science, 34, 883-907, 10.1016/s0021-8502(03)00052-1, 2003.

Han, Y., Lü, D., Rao, R., and Wang, Y.: Determination of the complex refractive indices of aerosol from aerodynamic particle size spectrometer and integrating nephelometer measurements, Applied Optics, 48, 4108-4117, 10.1364/AO.48.004108, 2009.

Hand, J. L., and Kreidenweis, S. M.: A New Method for Retrieving Particle Refractive Index and Effective Density from Aerosol Size Distribution Data, Aerosol Sci. Technol., 36, 1012-1026, 10.1080/02786820290092276, 2002.

Hänel, G.: REAL PART OF MEAN COMPLEX REFRACTIVE INDEX AND MEAN DENSITY OF SAMPLES OF ATMOSPHERIC AEROSOL PARTICLES, Tellus, 20, 371-&, 10.3402/tellusa.v20i3.10016, 1968.

Hu, M., Peng, J., Sun, K., Yue, D., Guo, S., Wiedensohler, A., and Wu, Z.: Estimation of size-resolved ambient particle density based on the measurement of aerosol number, mass, and chemical size distributions in the winter in Beijing, Environ Sci Technol, 46, 9941-9947, 10.1021/es204073t, 2012.

Kuang, Y., Zhao, C. S., Tao, J. C., and Ma, N.: Diurnal variations of aerosol optical properties in the North China Plain and their influences on the estimates of direct aerosol radiative effect, Atmos. Chem. Phys., 15, 5761-5772, 10.5194/acp-15-5761-2015, 2015.

Kuang, Y., Zhao, C. S., Tao, J. C., Bian, Y. X., and Ma, N.: Impact of aerosol hygroscopic growth on the direct aerosol radiative effect in summer on North China Plain, Atmospheric Environment, 147, 224-233, 2016.

Levoni, C., Cervino, M., Guzzi, R., and Torricella, F.: Atmospheric aerosol optical properties: a database of radiative characteristics for different components and classes, Appl Opt, 36, 8031-8041, 1997.

Lide, D. R.: Handbook of Chemistry and Physics, 86th Edition Edited(National Institute of Standards and Technology), Journal of the American Chemical Society, 128, 5585-5585, 10.1021/ja059868l, 2006.

Liu, H. J., Zhao, C. S., Nekat, B., Ma, N., Wiedensohler, A., van Pinxteren, D., Spindler, G., Müller, K., and Herrmann, H.: Aerosol hygroscopicity derived from size-segregated chemical composition and its parameterization in the North China Plain, Atmospheric Chemistry and Physics, 14, 2525-2539, 10.5194/acp-14-2525-2014, 2014.

Liu, Y., and Daum, P. H.: Relationship of refractive index to mass density and self-consistency of mixing rules for multicomponent mixtures like ambient aerosols, Journal of Aerosol Science, 39, 974-986, 10.1016/j.jaerosci.2008.06.006, 2008.

Ma, N., Zhao, C. S., Nowak, A., Müller, T., Pfeifer, S., Cheng, Y. F., Deng, Z. Z., Liu, P. F., Xu, W. Y., Ran, L., Yan, P., Göbel, T., Hallbauer, E., Mildenberger, K., Henning, S., Yu, J., Chen, L. L., Zhou, X. J., Stratmann, F., and Wiedensohler, A.: Aerosol optical properties in the North China Plain during HaChi campaign: an in-situ optical closure study, Atmos. Chem. Phys., 11, 5959-5973, 10.5194/acp-11-5959-2011, 2011.

Moise, T., Flores, J. M., and Rudich, Y.: Optical properties of secondary organic aerosols and their changes by chemical processes, Chemical Reviews, 115, 4400-4439, 2015.

421 Müller, T., Laborde, M., Kassell, G., and Wiedensohler, A.: Design and performance of a three-
422 wavelength LED-based total scatter and backscatter integrating nephelometer, Atmos. Meas. Tech., 4,
423 1291-1303, 10.5194/amt-4-1291-2011, 2011.
424 Peng, J., Hu, M., Guo, S., Du, Z., Zheng, J., Shang, D., Levy Zamora, M., Zeng, L., Shao, M., Wu, Y.-
425 S., Zheng, J., Wang, Y., Glen, C. R., Collins, D. R., Molina, M. J., and Zhang, R.: Markedly enhanced
426 absorption and direct radiative forcing of black carbon under polluted urban environments,
427 Proceedings of the National Academy of Sciences, 113, 4266-4271, 10.1073/pnas.1602310113, 2016.
428 Qiao, K., Wu, Z., Pei, X., Liu, Q., Shang, D., Zheng, J., Du, Z., Zhu, W., Wu, Y., Lou, S., Guo, S.,
429 Chan, C. K., Pathak, R. K., Hallquist, M., and Hu, M.: Size-resolved effective density of submicron
430 particles during summertime in the rural atmosphere of Beijing, China, Journal of Environmental
431 Sciences, 10.1016/j.jes.2018.01.012, 2018.
432 Ricchiazzi, P., Yang, S., Gautier, C., and Sowle, D.: SBDART: A Research and Teaching Software
433 Tool for Plane-Parallel Radiative Transfer in the Earth's Atmosphere, Bulletin of the American
434 Meteorological Society, 79, 2101-2114, 10.1175/1520-0477(1998)079<2101:sarats>2.0.co;2, 1998.
435 Seinfeld, J. H., Pandis, S. N., and Noone, K.: Atmospheric Chemistry and Physics: From Air Pollution
436 to Climate Change, Environment Science & Policy for Sustainable Development, 40, 26-26, 1998.
437 Stelson, A. W.: Urban aerosol refractive index prediction by partial molar refraction approach,
438 Environ.sci.technol, 24:11, 1676-1679, 1990.
439 Tao, J. C., Zhao, C. S., Ma, N., and Liu, P. F.: The impact of aerosol hygroscopic growth on the single-
440 scattering albedo and its application on the NO2 photolysis rate coefficient, Atmos. Chem. Phys., 14,
441 12055-12067, 10.5194/acp-14-12055-2014, 2014.
442 Wex, H., Neusüß, C., Wendisch, M., Stratmann, F., Koziar, C., Keil, A., Wiedensohler, A., and Ebert,
443 M.: Particle scattering, backscattering, and absorption coefficients: An in situ closure and sensitivity
444 study, Journal of Geophysical Research: Atmospheres, 107, LAC 4-1-LAC 4-18,
445 10.1029/2000jd000234, 2002.
446 Yue, G. K., Poole, L. R., Wang, P. H., and Chiou, E. W.: STRATOSPHERIC AEROSOL ACIDITY,
447 DENSITY, AND REFRACTIVE-INDEX DEDUCED FROM SAGE-II AND NMC
448 TEMPERATURE DATA, J Geophys Res-Atmos, 99, 3727-3738, 10.1029/93jd02989, 1994.

Zarzana, K. J., Cappa, C. D., and Tolbert, M. A.: Sensitivity of Aerosol Refractive Index Retrievals Using Optical Spectroscopy, Aerosol Sci. Technol., 48, 1133-1144, 10.1080/02786826.2014.963498, 2014.

Zhang, G., Bi, X., Qiu, N., Han, B., Lin, Q., Peng, L., Chen, D., Wang, X., Peng, P., apos, an, Sheng, G., and Zhou, Z.: The real part of the refractive indices and effective densities for chemically segregated ambient aerosols in Guangzhou measured by a single-particle aerosol mass spectrometer, Atmospheric Chemistry and Physics, 16, 2631-2640, 10.5194/acp-16-2631-2016, 2016.

Zhao, G., Zhao, C., Kuang, Y., Tao, J., Tan, W., Bian, Y., Li, J., and Li, C.: Impact of aerosol hygroscopic growth on retrieving aerosol extinction coefficient profiles from elastic-backscatter lidar signals, Atmospheric Chemistry and Physics, 17, 12133-12143, 10.5194/acp-17-12133-2017, 2017.

Zhao, G., Zhao, C., Kuang, Y., Bian, Y., Tao, J., Shen, C., and Yu, Y.: Calculating the aerosol asymmetry factor based on measurements from the humidified nephelometer system, Atmospheric Chemistry and Physics, 18, 9049-9060, 10.5194/acp-18-9049-2018, 2018a.

Zhao, G., Zhao, C., Zhao, W., and Hello, W.: Method to measure the size-resolved real part of aerosol refractive index, Atmos. Meas. Tech. Discuss., 2018, 1-20, 10.5194/amt-2018-399, 2018b.

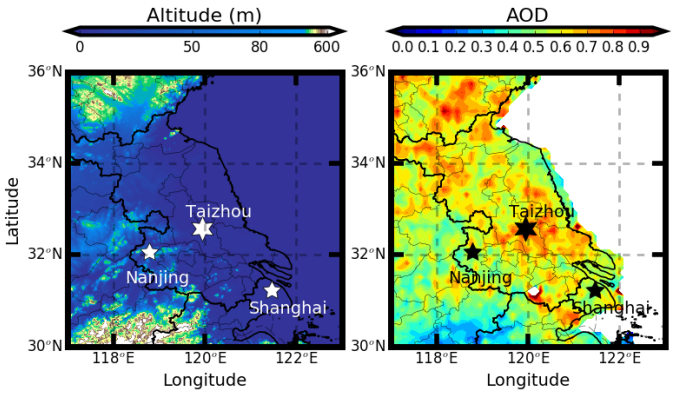

466

467 **Figure 1:** Measurement site of Taizhou (marked with stars). Filled colors represent (a) the

468 topography of the Jianghuai Plain. (b) the average aerosol optical depth at 550nm during the year of

469 2017 from Moderate Resolution Imaging Spectroradiometer onboard satellite Aqua.

470

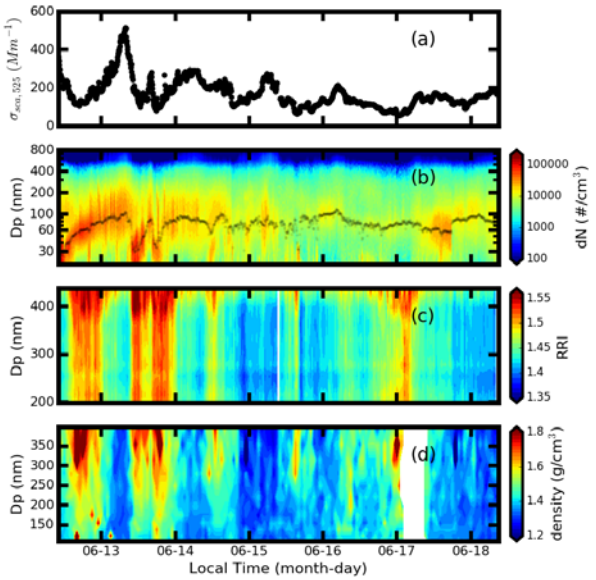

Figure 2. Time series of the measured (a) size-resolved RRI in filled color, σ_{sca} at 525nm in black dotted line and (b) the size-resolved ρ_{eff}.

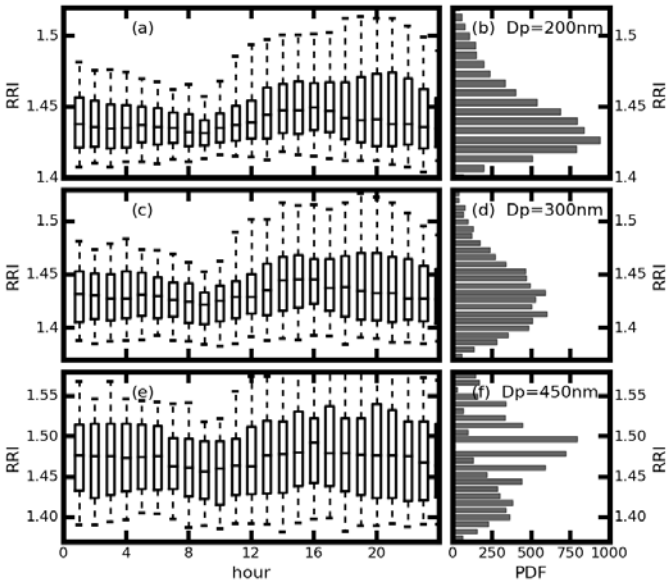

Figure 3. Daily variations of the RRI (a), (c) (e), and the probability distribution of the measured RRI (b), (d) (f) for the (a), (b) 200 nm, (c), (d) 300 nm, and (e), (f) 450nm aerosol respectively. The box and whisker plots represent the 5^{th}, 25^{th}, 75^{th} and 95^{th} percentiles.

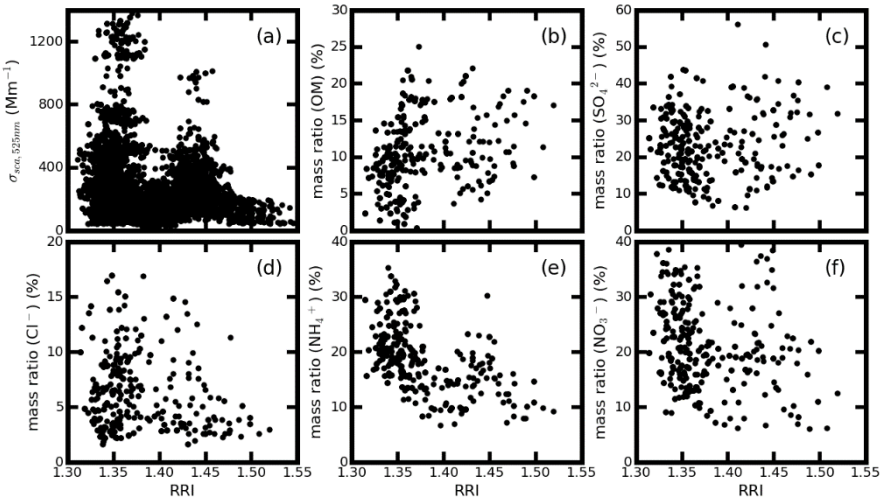

Figure 4. Comparison the measured RRI at 300nm with the measured (a) σ_{sca} at 525nm, mass fraction of (b) OM, (c) SO_4^{2-}, (d) Cl^-, (e) NH_4^+ and (f) NO_3^-.

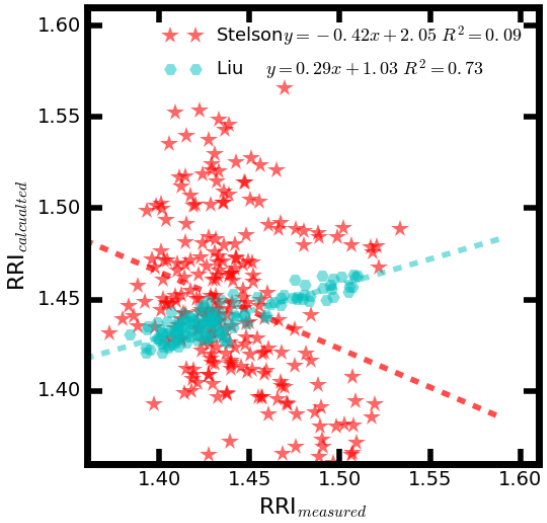

Figure 5. Comparison between the measured RRI and calculated RRI using the main aerosol chemical component from Stelson (1990) (in red star) and parameterization scheme proposed by Liu and Daum (2008) (in cyan hexagon).

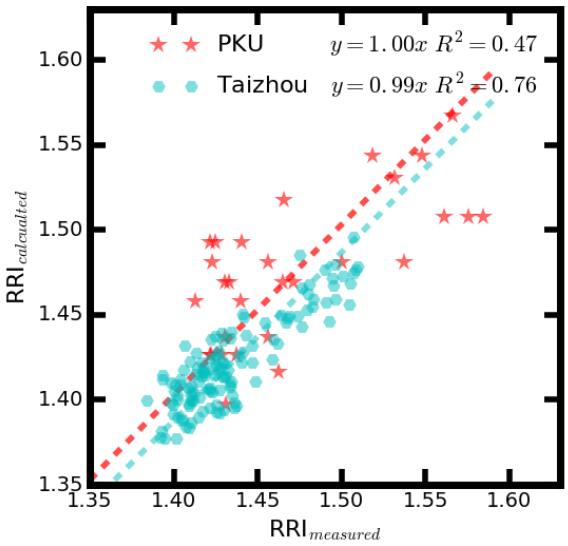

Figure 6. Comparison between the measured and calculated RRI for different at PKU (in red star) and Taizhou (in cyan hexagon) station.

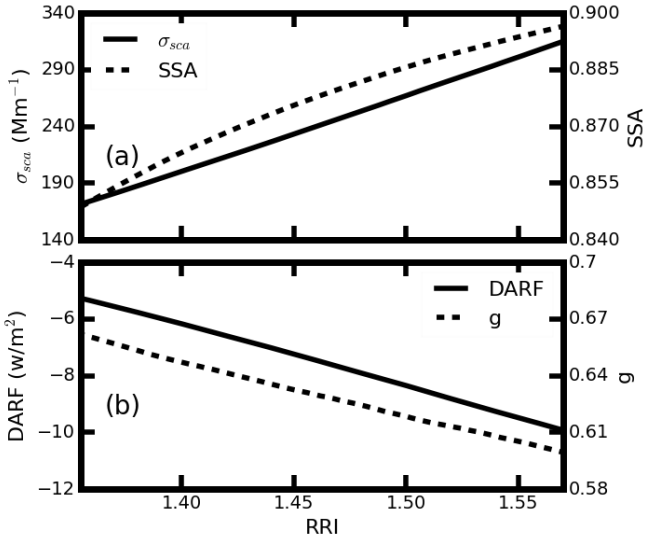

Figure 7. Variations of the estimated (a) σ_{sca} in solid line, SSA in dotted line, (b) g in dotted line, and DARF in solid line for different aerosol RRI.